

MERGING BINARY BLACK HOLES FROM YOUNG AND OLD MASSIVE STAR CLUSTERS

SOURAV CHATTERJEE¹, CARL L. RODRIGUEZ^{1,2}, VICKY KALOGERA¹, AND FREDERIC A. RASIO¹

¹Center for Interdisciplinary Exploration & Research in Astrophysics (CIERA)

Physics & Astronomy, Northwestern University, Evanston, IL 60202, USA

sourav.chatterjee@northwestern.edu

and

²MIT-Kavli Institute for Astrophysics and Space Research

77 Massachusetts Avenue, 37-664H, Cambridge, MA 02139, USA

ABSTRACT

Star clusters are efficient factories of binary black hole (BBH) mergers at low redshifts ($z < 0.2$). Using numerical models of star clusters spanning a wide range in stellar metallicities (Z) we study the effects of a parent cluster’s metallicity on the masses of BBHs merging in the local universe. We connect BBH merger times (t_{delay}) obtained from models of a given metallicity to the corresponding merger redshifts using a distribution of formation epochs for clusters of that stellar metallicity derived based on the cosmological star formation rate and metallicity evolution. We find that the mass distributions for BBHs merging in $z < 0.2$ can have significant overlap even when created in clusters of widely different stellar metallicities. This makes it hard to infer metallicity from the masses of individual merging BBHs. As the cluster metallicity decreases, the peaks and distributions for masses of its BBHs merging in $z < 0.2$ move to higher values, but for $Z/Z_{\odot} \lesssim 0.05$ they become insensitive to the cluster metallicity. We compare the intrinsic mass distributions for BBHs merging in $z < 0.2$ from our models with those observed. Masses of LVT151012 and GW151226 are similar to the peaks of the intrinsic mass distributions for models with $Z/Z_{\odot} = 0.25$ and 0.75 , and are within 1σ for models with $Z/Z_{\odot} \leq 0.25$ and $Z/Z_{\odot} \geq 0.5$, respectively. GW150914 is more massive (beyond 1σ) than typical BBHs merging in $z < 0.2$ even for the lowest metallicity ($Z/Z_{\odot} = 0.005$) clusters we consider, but is within 2σ of the intrinsic mass distributions from clusters with $Z/Z_{\odot} \leq 0.05$. Of course, accounting for aLIGO detectability would push the intrinsic distributions towards higher masses, hence the *detection* of merging BBHs as massive as GW150914 would be less rare. Since cluster dynamics typically increases BBH masses via exchange encounters relative to what could form in isolation, mergers of BBHs as massive as GW150914 in $z < 0.2$ is likely intrinsically rare in general.

Keywords: black hole physics—gravitational waves—methods: numerical—methods: statistical—globular clusters: general—galaxies: star clusters: general

1. INTRODUCTION

Detection of GWs from merging black hole (BH) binaries has rejuvenated widespread interest in understanding the astrophysical implications and the origins of BBHs (Abbott et al. 2016d,c,a). Current theoretical estimates indicate that detectable BBH merger events may be rather frequent, few–500 Gpc^{−3}yr^{−1}, with large uncertainties depending on model assumptions and uncertainties in BH physics (e.g., Ziosi et al. 2014; Dominik et al. 2015; Belczynski et al. 2016b; Rodriguez et al. 2015, 2016a; Chatterjee et al. 2016; Abbott et al. 2016b; Askar et al. 2016; Dvorkin et al. 2016; Mandel & de Mink 2016; de Mink & Mandel 2016). In the first observing run itself, the advanced LIGO observatories (aLIGO) have detected GW signals from two BBH mergers and a lower significance ‘trigger’ event (Abbott et al. 2016d,c,b). These detections already show a large diversity in the masses of merging BBHs in the

local universe: the chirp masses (M_{chirp}) at source for GW150914, LVT151012, and GW151226 are 28_{-2}^{+2} , 15_{-1}^{+1} , and $8.9_{-0.3}^{+0.3}$, respectively.

Broadly speaking, two major channels have been proposed for BBH formation and subsequent merger. High-mass stellar binaries may evolve in isolation to create merging BBHs, for example, by going through a specific sequence of events involving low-kick supernovae (SNe) and common envelope (CE) evolution (e.g., Dominik et al. 2012, 2013, 2015; Belczynski et al. 2014, 2016b; Kowalska-Leszczynska et al. 2015; Belczynski et al. 2016a), and via chemically homogeneous evolution of tidally distorted binaries (e.g., Mandel & de Mink 2016).

Alternatively, merging BBHs could be produced dynamically at the centers of dense star clusters (e.g., Ziosi et al. 2014; Rodriguez et al. 2015, 2016a). The process involved here is dramatically different from BBH forma-

tion in isolation. A negligible fraction of BBHs formed in dense massive star clusters are primordial, and none with merger delay times ≥ 1 Gyr are composed of BHs formed from stars that were born in that binary (e.g., [Rodriguez et al. 2016a](#); [Chatterjee et al. 2016](#)). As massive stellar binaries evolve in dense star clusters, even if they were initially hard, mass loss from stellar winds and compact object formation can make these binaries soft. Consequently, stellar encounters and natal kicks during BH formation disrupt these primordial binaries (e.g., [Chatterjee et al. 2016](#)). Single BHs dynamically acquire other BH companions via, e.g., three-body binary formation and binary-mediated exchange interactions which preferentially insert the relatively more massive BHs into a binary ejecting a less massive non-BH member from it (e.g., [Heggie & Hut 2003](#); [Chatterjee & Tan 2012](#); [Morscher et al. 2015](#); [Rodriguez et al. 2016b](#); [Chatterjee et al. 2016](#)).

While several studies have modeled BBH formation in isolation for a wide range in metallicities taking into account the cosmological evolutions of the star formation rate (SFR) and metallicity (e.g., [Belczynski et al. 2016a](#); [Dvorkin et al. 2016](#); [de Mink & Mandel 2016](#)), due to primarily the computational cost, numerical studies of dynamically formed BBHs have so far restricted themselves to either a narrow range in metallicities and ages with values similar to the majority of the Galactic globular clusters (GGCs) (e.g., [Rodriguez et al. 2015, 2016a](#); [Chatterjee et al. 2016](#)) or to low-mass (initial $N \sim 5 \times 10^3$), young (~ 100 Myr) star clusters (e.g., [Ziosi et al. 2014](#)). These studies also assumed that all model clusters formed roughly at the same epoch, e.g., $\simeq 12$ Gyr ago in case of GCs, to obtain the redshifts of BBH mergers from t_{delay} found in the models (e.g., [Rodriguez et al. 2016a](#); [Antonini et al. 2016](#); [Chatterjee et al. 2016](#)). This of course is a simplification. Stars form with wide ranges in metallicities at any redshift (e.g., [Madau & Dickinson 2014](#)). Massive star clusters are observed with a large range in ages and metallicities, for example, in M51, M101, and in the LMC (e.g., [Bastian et al. 2005](#); [Barmby et al. 2006](#); [Scheepmaker et al. 2007](#)). Even for the GGCs, the metallicity distribution has a long tail extending to Z_{\odot} ([Harris 1996](#)).

Here we relax past assumptions and consider BBH formation and merger in clusters spanning a wide range in stellar metallicities and metallicity-dependent distributions of cluster-formation redshifts. Our goal is to study the effects of star cluster metallicity and current age on the production rate, and the detectable properties (including mass and eccentricity) of BBH mergers. In §2 we describe our numerical setup. In §3 we show the key results. We conclude in §4.

2. NUMERICAL MODELS

We use our Hénon-type Monte Carlo cluster dynamics code **CMC** to model star clusters. **CMC** includes all physical processes relevant to study BBH production, dynamical evolution, and mergers in star clusters ([Joshi](#)

et al. 2000, 2001; [Fregeau et al. 2003](#); [Fregeau & Rasio 2007](#); [Chatterjee et al. 2010](#); [Umbreit et al. 2012](#); [Pattabiraman et al. 2013](#)). The initial structural properties are guided by those of the observed young massive clusters, thought to be similar in properties (except metallicity) to the progenitors of today’s GCs ([Scheepmaker et al. 2007](#); [Chatterjee et al. 2010, 2013](#)). We use seven different metallicities spanning a large range, namely $Z/Z_{\odot} = 0.005, 0.025, 0.05, 0.25, 0.5, 0.75$, and 1. Since we focus on studying the effects of star cluster metallicity on BBH mergers, we fix all other initial properties of our model clusters in the main set: all models initially have $N = 8 \times 10^5$ single/binary stars. The initial positions and velocities are assigned following a King profile with $w_0 = 5$. The initial virial radius $r_v = 2$ pc. The initial stellar masses (primary mass, M_p , in case of a binary) are drawn from the IMF given in [Kroupa \(2001\)](#) between 0.08 and $150 M_{\odot}$. The initial binary fraction is $f_b = 10\%$. We randomly select 10% of all stars to be binaries. The secondary masses (M_s) are drawn from a uniform distribution between $0.08/M_p$ and 1. The initial orbital periods for binaries are flat in logarithmic intervals, and the eccentricities (e) are thermal. The single and binary stellar evolution is done using the SSE and BSE software ([Hurley et al. 2000, 2002](#)) updated with new prescriptions for stellar winds (e.g., [Vink et al. 2001](#)) and a fallback-dependent natal kick distribution for BHs (e.g., [Belczynski et al. 2002](#); [Fryer et al. 2012](#)). To improve statistics we repeat each model using different seeds (Table 1).

We create two additional sets of models with $Z/Z_{\odot} = 0.05$ by varying the initial N and r_v to study their effects. In one set we change the initial r_v to 1 pc. In the other we vary the initial N to 2×10^5 and 2×10^6 . Relevant model properties are summarized in Table 1.

3. RESULTS

Merging BBHs decrease in mass with increasing metallicity, a direct consequence of the metallicity-dependence of the BH mass spectrum at formation (Fig. 1; [Belczynski et al. 2010](#)). Merging BBHs also decrease in mass as t_{delay} increases. This is because clusters form and dynamically process higher-mass BBHs first, followed by less massive ones due to mass segregation ([Breen & Heggie 2013](#); [Morscher et al. 2015](#)). Moreover, higher-mass BBHs merge faster due to GW radiation ([Peters 1964](#)).

Of all BBH mergers within a Hubble time, the fraction of in-cluster mergers varies from 0.3% from our highest-metallicity models ($Z/Z_{\odot} = 1$) to 5% from our lowest-metallicity models ($Z/Z_{\odot} = 0.005$). The majority of all BBHs merge long after they are ejected from the cluster predominantly via dynamical scattering at the cluster center. At most about 16% of all mergers involve merging of BHs whose progenitors were initially members of the same binary. Even for these, either the BHs or their progenitors have had at least one strong encounter (typically many), such as binary-mediated scattering, and

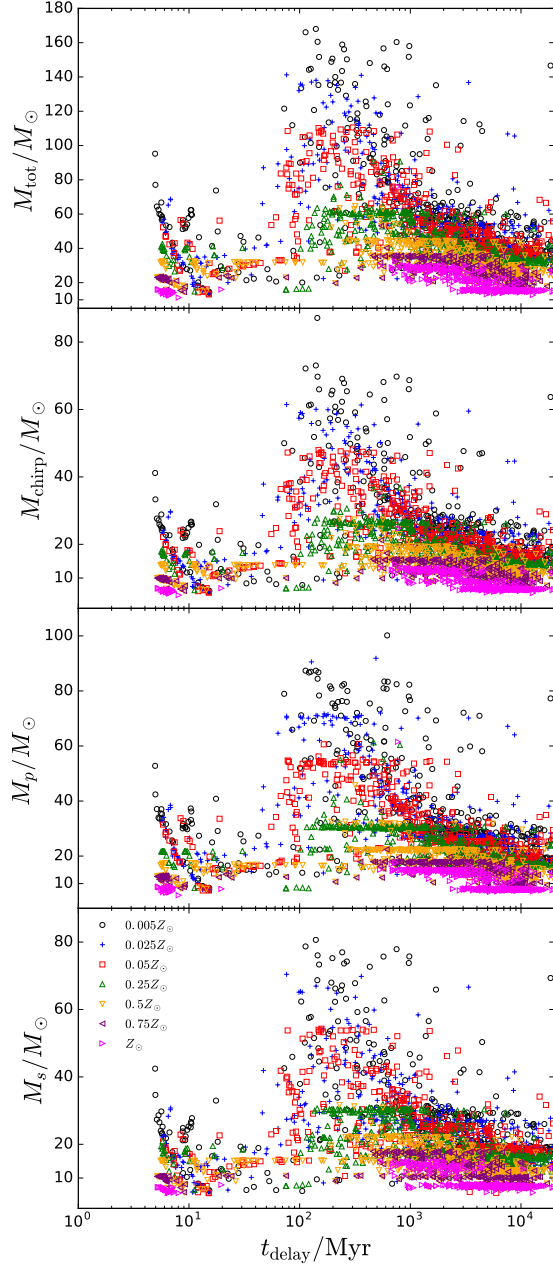


Figure 1. t_{delay} vs mass for BBH mergers in our models with different metallicities. t_{delay} is the time of BBH merger from $t = 0$ for the cluster. Black (circle), blue (plus), red (square), green (triangle-up), orange (triangle-down), purple (triangle-left), and magenta (triangle-right) denote BBH mergers from models with $Z/Z_{\odot} = 0.005, 0.025, 0.05, 0.25, 0.5, 0.75$, and 1 , respectively. Top to bottom, the panels show the M_{tot} , M_{chirp} , M_p , and M_s for all BBH mergers with $t_{\text{delay}} \leq 20$ Gyr. BBH mergers from lower-metallicity clusters are more massive, a consequence of the Z -dependence of the BH mass function at formation (e.g., Belczynski et al. 2010). Heavier BBH mergers have shorter t_{delay} for any Z , a consequence of how BHs are dynamically processed inside clusters and the mass dependence of the inspiral time via GW radiation from a given initial separation (Peters 1964). The apparent over-density of mergers at specific BBH masses for a given metallicity is due to spikes in the BH MF at formation, expected from the progenitor-to-remnant mass relation (Belczynski et al. 2010).

physical collisions before they merge. Massive stars and resulting BHs quickly mass segregate to the densest part of the cluster. Even if the initial binary is not disrupted due to natal kicks or strong scattering, their primordial orbital properties are significantly altered due to dynamics (similar conclusions in, e.g., Chatterjee et al. 2016; Rodriguez et al. 2016b).

3.1. Merger time delay vs redshift

In order to compare the properties of BBH mergers in our models with those observed, we need to connect t_{delay} to redshift. Past studies focusing on BBH mergers from GCs assumed that all GCs are ~ 12 Gyr old, thus, there is a one-to-one correspondence between t_{delay} of mergers from models and redshift. In reality, clusters of a given stellar metallicity may have a wide range of formation redshifts (e.g., Madau & Dickinson 2014). We closely follow the approach of Belczynski et al. (2016a) and adopt cosmological constraints for $\text{SFR}(z)$ and $Z(z)$ (Madau & Dickinson 2014) to infer the redshift-distribution of formation for clusters with a given stellar metallicity. We assume

$$\text{SFR}(z) = 0.015 \frac{(1+z)^{2.7}}{1 + \{(a+z)/2.9\}^{5.6}} M_{\odot} \text{Mpc}^{-3} \text{yr}^{-1}. \quad (1)$$

$\text{SFR}(z)$ peaks at $z \simeq 2$, corresponding to a look-back time $t_{\text{lb}} \simeq 10$ Gyr, and decreases sharply on either side. For example, $\text{SFR}(z)$ drops by a factor of 5 from its peak value by $z = 0.24$ ($t_{\text{lb}} \simeq 3$ Gyr) and $z = 5.4$ ($t_{\text{lb}} \simeq 12$ Gyr). Chemical enrichment of the universe depends on the SFR. The mean stellar metallicity, \bar{Z} , is given by

$$\log \bar{Z}(z) = K + \log \left(\frac{y(1-R)}{\rho_b} \int_z^{20} \frac{97.8 \times 10^{10} \text{SFR}(z')}{H_0 E(z')(1+z')} dz' \right) \quad (2)$$

(Belczynski et al. 2016a, their Eq. 2). $R = 0.27$ is the mass fraction of a generation of stars that remixes into the interstellar medium, $y = 0.019$ is the net metal production, $\rho_b = 2.77 \times 10^{11} \Omega_b h_0^2 M_{\odot} \text{Mpc}^{-3}$ is the baryon density, and $E(z) = \sqrt{\Omega_M(1+z)^3 + \Omega_k(1+z)^2 + \Omega_{\Lambda}}$.¹ We adopt the normalization constant $K = 1.30749$ to obtain $\bar{Z} = 0.001$ and 0.02 for $t_{\text{lb}} \simeq 12$ and 5 Gyr, respectively, guided by the typical ages and metallicities of the GGCs and the Sun. The exact adopted value of K (within constraints) does not affect our results significantly.

The probability distribution function (PDF) for the redshifts of formation for clusters of a given metallicity Z' is,

$$f(z)_{Z'} = \int_{Z=0.9Z'}^{1.1Z'} \int_{z'=0}^{20} \text{SFR}(z') f'(Z)_{z'} dz' dZ, \quad (3)$$

where, $f'(Z)_z$ is assumed to be lognormal with $\sigma = 0.5$ dex and mean $= \bar{Z}(z)$, given by Eq. 2 (Belczynski et al.

¹ We assume $\Omega_b = 0.045$, $h_0 = 0.7$, $\Omega_{\Lambda} = 0.7$, $\Omega_M = 0.3$, $\Omega_k = 0$, and $H_0 = 70 \text{ km s}^{-1} \text{Mpc}^{-1}$.

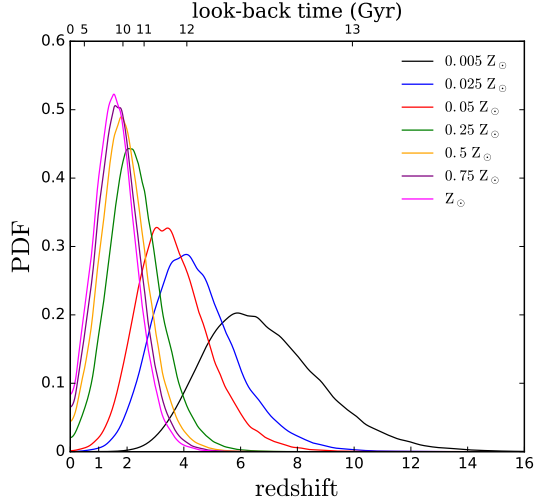


Figure 2. PDF for the redshift of formation (z_{form}) for star clusters of different stellar metallicities (Eq. 3). Black, blue, red, green, orange, purple, and magenta denote cluster metallicities $Z/Z_{\odot} = 0.005, 0.025, 0.05, 0.25, 0.5, 0.75$, and 1 , respectively. Look-back times corresponding to z_{form} are also shown for reference.

2016a). We evaluate $f(z)_{Z'}$ in the following way. We randomly generate 10^5 redshift values between 0 and 20 weighted by $\text{SFR}(z)$ (Eq. 1). For each draw of redshift we calculate \bar{Z} and randomly generate 10^2 metallicity values from $f'(Z)_z$. Thus we generate a database of 10^7 redshift-metallicity pairs. We then collect all redshift values corresponding to metallicities within $Z' \pm 0.1Z'$. The PDF $f(z)_{Z'}$ is then obtained from these selected redshift values using a gaussian kernel density estimator (KDE) with bandwidth determined by Scott's method (Scott 1992). We find that $f(z)_Z$ can be distributed across a large range in redshift, especially for clusters with low stellar metallicities. Furthermore, due to the sharp peak of $\text{SFR}(z)$ at $z \simeq 2$, the modes of $f(z)_Z$, even for the highest metallicities we consider, are pushed towards $z = 2$ (Fig. 2, Table 1).

3.2. Properties of BBH mergers within $0 \leq z \leq 1$

We take 500 random draws of the redshift of cluster formation (z_{form}) from $f(z)_{Z'}$ (Eq. 3; Fig. 2) for clusters of a given metallicity, Z' . For each model of a particular metallicity and for each draw of z_{form} we map the window of interest for BBH merger redshifts, Δz (e.g., $0 \leq z \leq 1$), to the corresponding window in t_{delay} , and collect all BBH mergers within Δz . This essentially acts as a sliding window of selection of BBH mergers from a cluster within Δz based on the distribution of that cluster's formation times. We create a multi-dimensional (redshift, M_p , and M_s) PDF from the selected BBH mergers from all cluster models of a given set of initial properties. We then draw a sample of 10^5 BBH mergers from this PDF to investigate the BBH merger properties for each metallicity.

Fig. 3 shows the distributions for M_{tot} , M_{chirp} , M_p ,

and M_s for the merging BBHs from clusters with seven different metallicities. The left panels show 1σ contours for BBH mergers in the mass-redshift plane. The right panels show the full mass distributions for merging BBHs within $z \leq 0.2$. For a given cluster metallicity, the 1σ contours encompass higher masses as the merger redshift increases. This simply is because the lower the t_{delay} (equivalent to higher redshift), the higher the mass of merging BBHs (Fig. 1).

The distributions for merging BBH masses, even from clusters of vastly different metallicities, show significant overlap for any $z \leq 1$ due to several competing effects and the wide range in cluster-formation redshifts for any metallicity, which makes inferring the metallicity of a particular merging BBH hard. Lower-metallicity clusters form higher-mass BBHs simply because BHs formed from lower-metallicity progenitors are heavier (e.g., Belczynski et al. 2010). However, lower-metallicity clusters have higher formation redshifts. Hence, a particular observation window in redshift corresponds to higher t_{delay} in lower-metallicity clusters, allowing only lower-mass merging BBHs into that redshift window (Fig. 1). Furthermore, for a given separation, heavier BBHs (formed in, e.g., lower-metallicity clusters) merge faster reducing t_{delay} . Due to these same reasons, the distributions and their peaks for BBH masses merging in $z \leq 0.2$ do not change significantly for any $Z/Z_{\odot} \leq 0.05$ (Fig. 3, Table 1).

The properties of the detected GW sources, GW150914, LVT151012, and GW151226 are shown in Fig. 3 for comparison. For simplicity we compare the intrinsic mass distributions of BBH mergers within, e.g., $z \leq 0.2$, with the source-frame M_{chirp} of the detected GW sources. M_{chirp} for LVT151012 and GW151226 are within 1σ of the M_{chirp} distributions for BBHs merging within $z \leq 0.2$ from models with $Z/Z_{\odot} \leq 0.25$ and $Z/Z_{\odot} \geq 0.5$, respectively. Moreover, M_{chirp} for LVT151012 and GW151226 line up perfectly with the peaks for $Z/Z_{\odot} = 0.25$ and 0.75 , respectively (Fig. 3, Table 1).

M_{chirp} for GW150914 is within 2σ of the M_{chirp} distributions for $Z/Z_{\odot} \leq 0.05$, but is higher than 1σ of the M_{chirp} distributions for any metallicities we consider. Since for $Z/Z_{\odot} \lesssim 0.05$, M_{chirp} distributions are not sensitive to the cluster metallicity, GW150914 is likely more massive than intrinsically typical BBHs merging in $z \leq 0.2$. Nevertheless, note that we do not consider aLIGO detectability in finding the mass distributions of merging BBHs. Accounting for detectability constraints of BBH mergers, especially from low-metallicity clusters, would significantly reduce and enhance low- and high-mass regions of the PDF, respectively (Rodriguez et al. 2016b). Hence, if detectability is accounted for, GW150914 might actually not be an outlier among detectable BBH mergers from low-metallicity, old clusters. For example, Rodriguez et al. (2016b) find that GW150914's M_{chirp} is within 1σ of the M_{chirp} distribution of BBHs merging in $z \leq 0.5$ from GCs

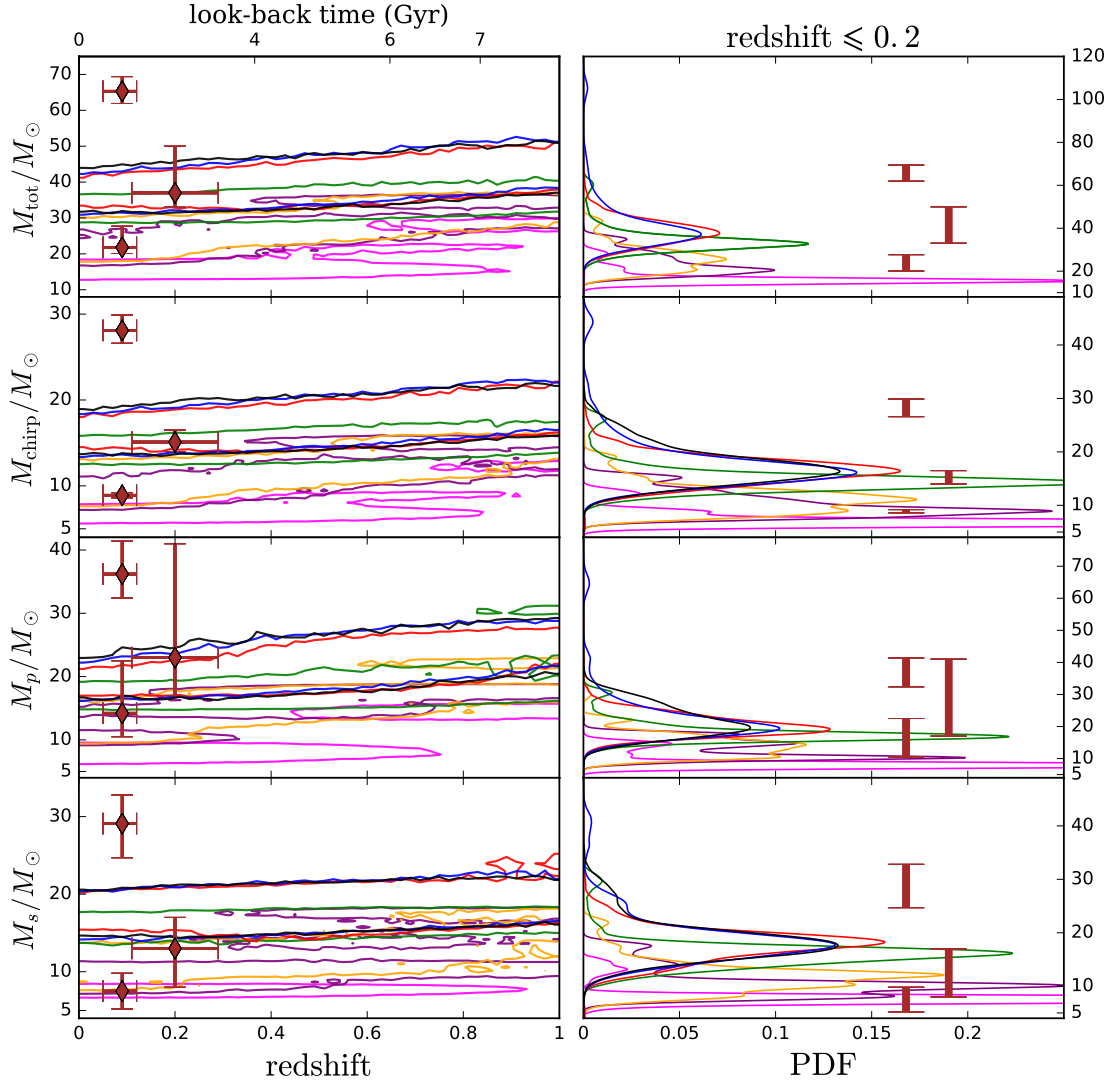


Figure 3. BBH merger masses and redshift. Top to bottom, the panels show M_{tot} , M_{chirp} , M_p and M_s for BBH mergers. Left panels show 1σ contours for BBH merger masses as a function of merger redshift. Right panels show the mass distributions for BBH mergers with $z \leq 0.2$. Redshift for BBH mergers are evaluated from t_{delay} in our models and the derived distributions of cluster formation redshifts (§3.1, Fig. 2). Black, blue, red, green, orange, purple, and magenta denote $Z/Z_{\odot} = 0.005, 0.025, 0.05, 0.25, 0.5, 0.75$, and 1 , respectively. Brown diamonds and error-bars denote the source-frame properties and 90% confidence intervals for the observed BBH mergers (Abbott et al. 2016b). Note that these distributions are intrinsic BBH properties without accounting for aLIGO detectability. The *detectable* distributions would be pushed towards higher masses, especially for low metallicities (e.g., Rodriguez et al. 2016b).

formed at $z \simeq 3.5$, if detectability is considered. Keeping this in mind, it is actually not surprising that the first ever detected GWs came from the merger of an intrinsically unusually massive BBH. BH dynamics in a star cluster increases BBH masses (via repeated exchange encounters) and t_{delay} (Chatterjee et al. 2016; in preparation) relative to BBHs formed in isolation. Thus, for a given metallicity and z_{form} , it is likely harder to create BBH mergers as massive as GW150914 in isolation in the local universe.

3.3. Variation due to initial cluster properties

Since all BBHs that form in star clusters and merge in the local universe are dynamically created, their properties also depend on the parent cluster’s dynamical properties in addition to its stellar metallicity. The escape speed of the cluster, set by the cluster mass, sets the separation of the binaries at ejection (recently Rodriguez et al. 2016a). The relaxation timescale (t_{relax}) controls the timescale for dynamical processing of BHs. Variations in initial N and r_v captures both of the above effects. While simulating a large grid of models with

large ranges in metallicity as well as large ranges in initial cluster properties is beyond the scope of this study, we vary the initial N and r_v for our models with $Z/Z_\odot = 0.05$ (§2) to investigate the effects of these changes.

The distributions of, e.g., M_{tot} and M_{chirp} for BBH mergers within $z \leq 0.2$ (and $z \leq 1$) from models with $Z/Z_\odot = 0.05$ overlap significantly with each other even when initial N is changed by an order of magnitude, and the initial r_v is changed by a factor of 2: the modes of the distributions for both M_{tot} and M_{chirp} are well within 1σ of each other (Fig. 4). Nevertheless, clusters with lower initial r_v processes through the BHs quicker due to their shorter t_{relax} . Hence, BBHs merging within, e.g., $z \leq 0.2$, are slightly less massive from clusters with initial $r_v = 1$ pc compared to those from clusters with initial $r_v = 2$ pc (Fig. 4, Table 1).

BBH masses merging at low redshifts do not seem to be sensitive to variations in initial N . On one hand, a higher- N cluster (keeping all else fixed) ejects BBHs that are tighter, thus decreasing t_{delay} (e.g., [Rodriguez et al. 2016a](#)). On the other hand, higher- N increases t_{relax} , resulting in slower dynamical processing of BHs and slower decrease of M_{chirp} with respect to t_{delay} (e.g., [Heggie & Hut 2003](#); [Breen & Heggie 2013](#); [Morscher et al. 2015](#)). These competing effects seem to make the distribution peaks for BBH masses merging in the local universe insensitive to the initial N of the host cluster. This trend of course should not be extrapolated to very low- N clusters that dissolve before significant dynamical processing of their BBHs.

In addition to masses, we follow the eccentricities of BBH orbits merging in $z \leq 1$ using the quadrupole approximated GW orbital evolution equations ([Peters 1964](#)) and find the e -distributions when the frequency of maximum GW power (f_{GW} ; [Wen 2003](#)) for these BBHs enter the aLIGO (10 Hz) and LISA (10^{-4} Hz) frequency bands. Similar to [Breivik et al. \(2016\)](#), we find that by the time BBHs (that merge in $z \leq 1$) reach $f_{\text{GW}} = 10$ Hz, they have very low $e \sim 10^{-7}$. Whereas, $e \sim 0.01$ – 0.4 for the same BBH orbits when $f_{\text{GW}} = 10^{-4}$ Hz.² We do not find any clear trends in the distributions of $\log e$ at these frequencies depending on the cluster metallicity, N or r_v in our models.

4. DISCUSSION

We have studied the effects of the parent cluster’s stellar metallicity (and metallicity-dependent age) on the masses of BBH mergers in the local universe. We have created detailed star cluster models spanning a wide range in stellar metallicities to represent the full population of massive clusters, both the GGCs and younger and more metal rich super star clusters. We derive the distribution of formation redshifts for a cluster of a given

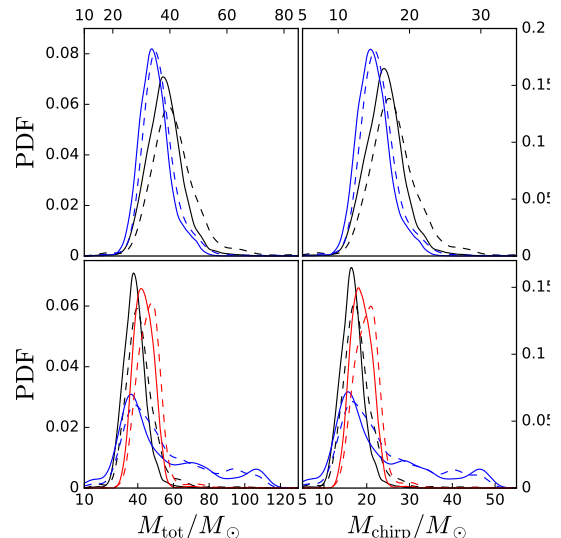


Figure 4. Distributions of M_{tot} (left) and M_{chirp} (right) for BBH mergers from clusters with different initial properties, but the same $Z/Z_\odot = 0.05$. Solid and dashed distributions denote mergers with $z \leq 0.2$ and $z \leq 1$, respectively. Top panels compare between BBH merger masses from clusters with initial $r_v = 1$ pc (blue) and 2 pc (black). Bottom panels compare between the same from clusters with initial $N = 2 \times 10^5$ (blue), 8×10^5 (black), and 2×10^6 (red). The distributions have significant overlap even when initial N is varied by an order of magnitude, and r_v is varied by a factor of two. All peaks are significantly within 1σ of each other (Table 1).

stellar metallicity based on the cosmological SFR and metallicity evolution (Eq. 3, Fig. 2). The t_{delay} for BBH mergers, directly obtained from our models, are converted to redshifts of BBH mergers based on the z_{form} distribution. Several trends emerge. For example, less massive BBHs have longer t_{delay} for any metallicity since star clusters dynamically form, process, and eject heavier BBHs earlier due to mass segregation (e.g., [Breen & Heggie 2013](#); [Morscher et al. 2015](#)). In addition, heavier BBHs merge faster from a given separation via GW radiation than less massive ones ([Peters 1964](#)). As a result, although BBHs with $M_{\text{chirp}} \geq 40 M_\odot$ are often created in low-metallicity clusters, they typically merge well before $z \sim 1$ (Fig. 1).

Lower-metallicity clusters typically have higher z_{form} . Hence, a BBH merger from a lower-metallicity cluster requires a longer t_{delay} to be in the local universe. While lower metallicity leads to the formation of heavier BBHs (e.g., [Fryer et al. 2012](#)), longer t_{delay} decreases merging BBH masses (Fig. 1). Competition between these two effects makes the mass distributions for BBHs merging in $z \leq 0.2$ insensitive to the parent cluster’s metallicity for $Z/Z_\odot \lesssim 0.05$. Above this metallicity, mass distributions of merging BBHs peak at lower masses as the metallicity increases. The distributions for merging BBH masses exhibit wide ranges, especially for low metallicities, where even the 1σ range in, e.g., M_{chirp} , can be $\simeq 50\%$ of the M_{chirp} at peak. This leads to significant overlap between these distributions from clusters

² We neglect hierarchical triples which contribute at $\sim 1\%$ level for clusters ([Antonini et al. 2016](#))

of widely different metallicities making it hard to predict the metallicities of individual merging BBHs.

We compare the intrinsic mass distributions of merging BBHs from our models to the masses of observed GW events. We find that M_{chirp} of GW150914 is not within 1σ of the intrinsic M_{chirp} distributions for BBHs merging in $z \leq 0.2$ for any metallicities we consider, but is within 2σ for mergers from clusters with $Z/Z_{\odot} \leq 0.05$. Since decreasing metallicity further does not change the M_{chirp} -distribution significantly and dynamically created BBHs are generally heavier than those produced in isolation for any given metallicity, mergers of BBHs as massive as GW150914 in $z \leq 0.2$ are likely intrinsically rare. Of course, accounting for detectability would push the intrinsic distributions towards higher masses making the *detection* of mergers like GW150914 less rare (Rodriguez et al. 2016b). M_{chirp} of LVT151012 is very similar to the peak of the distribution from clusters with $Z/Z_{\odot} = 0.25$, and is within 1σ of the distributions from all clusters with $Z/Z_{\odot} \leq 0.25$. M_{chirp} of GW151226 is within 1σ of the distributions from clusters with $Z/Z_{\odot} \geq 0.5$ and is very close to the peak from clusters of $Z/Z_{\odot} = 0.75$.

The actual mass distributions can potentially change

depending on initial cluster properties that directly affect t_{relax} in a cluster, such as initial N and r_v , since all timescales relevant for the dynamical processing of BHs in a cluster depend on t_{relax} . We find that the mass distributions for BBHs merging in the local universe are not very sensitive to the initial N (Fig. 4) even when N is varied over an order of magnitude. A change in r_v by a factor of 2 shifts the mass distributions to slightly lower values (Fig. 4, Table 1). This indicates that the stellar metallicity and metallicity-dependent age of the parent cluster are likely the most important properties to determine the peaks and distributions of BBH masses merging in the local universe. This of course is always true for BBHs formed in isolation.

This work was supported by NSF Grant AST-1312945, NSF Grant PHY-1307020, and NASA Grant NNX14AP92G. CR is grateful for the hospitality of the Kavli Institute for Theoretical Physics, supported by NSF Grant PHY11-25915, and is supported at MIT by a Pappalardo Fellowship in Physics. VK and FAR also acknowledge support from NSF Grant PHY-1066293 at the Aspen Center for Physics.

REFERENCES

- Abbott, B. P., Abbott, R., Abbott, T. D., et al. 2016a, The Astrophysical Journal Letters, 818, L22
- . 2016b, arXiv:1606.04856
- . 2016c, Phys. Rev. Lett., 116, 241103
- . 2016d, Phys. Rev. Lett., 116, 061102
- Antonini, F., Chatterjee, S., Rodriguez, C. L., et al. 2016, ApJ, 816, 65
- Askar, A., Szkudlarek, M., Gondek-Rosińska, D., Giersz, M., & Bulik, T. 2016, arXiv:1608.02520
- Barmby, P., Kuntz, K. D., Huchra, J. P., & Brodie, J. P. 2006, AJ, 132, 883
- Bastian, N., Gieles, M., Lamers, H. J. G. L. M., Scheepmaker, R. A., & de Grijs, R. 2005, A&A, 431, 905
- Belczynski, K., Buonanno, A., Cantiello, M., et al. 2014, ApJ, 789, 120
- Belczynski, K., Dominik, M., Bulik, T., et al. 2010, ApJL, 715, L138
- Belczynski, K., Holz, D. E., Bulik, T., & O’Shaughnessy, R. 2016a, Nature, 534, 512
- Belczynski, K., Kalogera, V., & Bulik, T. 2002, ApJ, 572, 407
- Belczynski, K., Repetto, S., Holz, D. E., et al. 2016b, ApJ, 819, 108
- Breen, P. G., & Hoggie, D. C. 2013, MNRAS, 432, 2779
- Breivik, K., Rodriguez, C. L., Larson, S. L., Kalogera, V., & Rasio, F. A. 2016, arXiv:1606.09558
- Chatterjee, S., Fregeau, J. M., Umbreit, S., & Rasio, F. A. 2010, ApJ, 719, 915
- Chatterjee, S., Rodriguez, C. L., & Rasio, F. A. 2016, arXiv:1603.00884
- Chatterjee, S., & Tan, J. C. 2012, ApJ, 754, 152
- Chatterjee, S., Umbreit, S., Fregeau, J. M., & Rasio, F. A. 2013, MNRAS, 429, 2881
- de Mink, S. E., & Mandel, I. 2016, MNRAS, 460, 3545
- Dominik, M., Belczynski, K., Fryer, C., et al. 2012, ApJ, 759, 52
- . 2013, ApJ, 779, 72
- Dominik, M., Berti, E., O’Shaughnessy, R., et al. 2015, ApJ, 806, 263
- Dvorkin, I., Vangioni, E., Silk, J., Uzan, J.-P., & Olive, K. A. 2016, MNRAS, 461, 3877
- Fregeau, J. M., Gürkan, M. A., Joshi, K. J., & Rasio, F. A. 2003, ApJ, 593, 772
- Fregeau, J. M., & Rasio, F. A. 2007, ApJ, 658, 1047
- Fryer, C. L., Belczynski, K., Wiktorowicz, G., et al. 2012, ApJ, 749, 91
- Harris, W. E. 1996, AJ, 112, 1487
- Hoggie, D., & Hut, P. 2003, The Gravitational Million-Body Problem: A Multidisciplinary Approach to Star Cluster Dynamics
- Hurley, J. R., Pols, O. R., & Tout, C. A. 2000, MNRAS, 315, 543
- Hurley, J. R., Tout, C. A., & Pols, O. R. 2002, MNRAS, 329, 897
- Joshi, K. J., Nave, C. P., & Rasio, F. A. 2001, ApJ, 550, 691
- Joshi, K. J., Rasio, F. A., & Portegies Zwart, S. 2000, ApJ, 540, 969
- Kowalska-Leszczynska, I., Regimbau, T., Bulik, T., Dominik, M., & Belczynski, K. 2015, A&A, 574, A58
- Kroupa, P. 2001, MNRAS, 322, 231
- Madau, P., & Dickinson, M. 2014, ARA&A, 52, 415
- Mandel, I., & de Mink, S. E. 2016, MNRAS, 458, 2634
- Morscher, M., Pattabiraman, B., Rodriguez, C., Rasio, F. A., & Umbreit, S. 2015, ApJ, 800, 9
- Pattabiraman, B., Umbreit, S., Liao, W.-k., et al. 2013, ApJS, 204, 15
- Peters, P. C. 1964, Physical Review, 136, 1224
- Rodriguez, C. L., Chatterjee, S., & Rasio, F. A. 2016a, PhRvD, 93, 084029
- Rodriguez, C. L., Haster, C.-J., Chatterjee, S., Kalogera, V., & Rasio, F. A. 2016b, ApJL, 824, L8
- Rodriguez, C. L., Morscher, M., Pattabiraman, B., et al. 2015, Physical Review Letters, 115, 051101
- Scheepmaker, R. A., Haas, M. R., Gieles, M., et al. 2007, A&A, 469, 925

- Scott, D. W. 1992, *Multivariate Density Estimation*
- Umbreit, S., Fregeau, J. M., Chatterjee, S., & Rasio, F. A. 2012, *ApJ*, 750, 31
- Vink, J. S., de Koter, A., & Lamers, H. J. G. L. M. 2001, *A&A*, 369, 574
- Wen, L. 2003, *ApJ*, 598, 419
- Ziosi, B. M., Mapelli, M., Branchesi, M., & Tormen, G. 2014, *MNRAS*, 441, 3703

Table 1. Star cluster models and BBH merger properties.

N (10^5)	M_i ($10^5 M_\odot$)	r_v (pc)	Z/Z_\odot	#	Cluster Formation Time		BBH Merger Properties					N_{merge}		
					z_{form}	t_{lb} (Gyr)	M_{tot} (M_\odot)	M_{chirp} (M_\odot)	M_{tot} (M_\odot)	M_{chirp} (M_\odot)	$\log e_1$		$\log e_{-4}$	
							$z \leq 0.2$		$z \leq 1$		$z \leq 1$		$z \leq 0.2$	$z \leq 1$
8	5	2	0.005	4	$6.2^{+1.9}_{-1.7}$	$12.6^{+0.3}_{-0.4}$	$37.7^{+8.4}_{-7.0}$	$16.4^{+3.5}_{-3.1}$	$39.8^{+9.4}_{-7.4}$	$17.3^{+3.9}_{-3.3}$	$-7.3^{+0.8}_{-0.8}$	$-2.0^{+0.8}_{-0.8}$	4^{+4}_{-1}	26^{+2}_{-5}
					$4.2^{+1.1}_{-1.4}$	$12.0^{+0.4}_{-0.9}$	$37.2^{+7.6}_{-6.8}$	$16.1^{+3.3}_{-2.9}$	$39.2^{+9.9}_{-6.5}$	$16.9^{+4.2}_{-3.8}$	$-7.3^{+1.1}_{-0.6}$	$-2.0^{+1.1}_{-0.5}$	4^{+5}_{-1}	24^{+7}_{-1}
					$3.4^{+1.1}_{-1.1}$	$11.6^{+0.5}_{-1.0}$	$37.6^{+5.9}_{-5.9}$	$16.4^{+2.5}_{-2.7}$	$39.6^{+7.7}_{-6.9}$	$17.1^{+3.4}_{-3.0}$	$-7.2^{+0.8}_{-0.7}$	$-1.9^{+0.8}_{-0.6}$	4^{+1}_{-2}	30^{+2}_{-12}
					$2.1^{+1.0}_{-0.7}$	$10.3^{+1.0}_{-1.5}$	$32.7^{+3.8}_{-3.8}$	$14.2^{+1.7}_{-1.7}$	$33.3^{+6.4}_{-4.4}$	$14.5^{+2.7}_{-1.9}$	$-7.0^{+1.1}_{-0.8}$	$-1.8^{+1.1}_{-0.6}$	6^{+1}_{-3}	22^{+3}_{-2}
20	12	2	0.05	4	$1.8^{+0.8}_{-0.7}$	$9.9^{+1.1}_{-1.9}$	$25.6^{+4.3}_{-6.9}$	$11.1^{+1.8}_{-3.0}$	$27.8^{+8.2}_{-5.8}$	$11.4^{+4.2}_{-2.0}$	$-6.5^{+0.8}_{-0.9}$	$-1.1^{+0.7}_{-0.2}$	3^{+2}_{-1}	24^{+1}_{-6}
					$1.6^{+0.8}_{-0.7}$	$9.6^{+1.3}_{-2.2}$	$20.5^{+6.5}_{-3.5}$	$8.9^{+2.6}_{-1.6}$	$28.5^{+7.0}_{-7.5}$	$10.9^{+2.4}_{-2.1}$	$-6.5^{+0.8}_{-0.9}$	$-1.1^{+0.2}_{-0.8}$	5^{+1}_{-3}	16^{+5}_{-1}
					$1.6^{+0.7}_{-0.8}$	$9.4^{+2.1}_{-2.5}$	$15.4^{+1.9}_{-1.7}$	$6.7^{+0.8}_{-0.8}$	$15.5^{+6.3}_{-2.2}$	$6.7^{+2.5}_{-0.8}$	$-7.0^{+1.1}_{-0.4}$	$-1.8^{+1.1}_{-0.2}$	8^{+2}_{-4}	40^{+1}_{-5}
					$3.4^{+1.1}_{-1.1}$	$11.6^{+0.5}_{-1.0}$	$32.9^{+4.8}_{-4.8}$	$14.1^{+2.2}_{-2.2}$	$33.9^{+6.1}_{-5.1}$	$14.5^{+2.9}_{-2.1}$	$-6.4^{+0.6}_{-1.1}$	$-1.0^{+0.5}_{-1.1}$	3^{+3}_{-1}	22^{+7}_{-1}
2	1	2	0.05	18	$3.4^{+1.1}_{-1.1}$	$11.6^{+0.5}_{-1.0}$	$41.8^{+7.2}_{-4.6}$	$17.9^{+3.4}_{-1.8}$	$48.3^{+4.2}_{-8.6}$	$21.0^{+1.8}_{-4.0}$	$-6.2^{+0.7}_{-1.1}$	$-0.6^{+0.5}_{-1.1}$	16^{+2}_{-6}	60^{+9}_{-1}
					37^{+30}_{-11}	$16^{+13}_{-4.8}$	39^{+26}_{-10}	17^{+11}_{-5}	$-6.7^{+0.8}_{-1.1}$	$-1.4^{+0.8}_{-1.1}$	0^{+4}_{-0}	3^{+1}_{-1}		

NOTE— M_i is the initial cluster mass. # denotes the number of models simulated with the same initial cluster properties. Cluster formation redshifts, z_{form} , and the equivalent look-back times, t_{lb} , are shown for clusters of particular metallicities (§3.1). We denote the eccentricities of BBH orbits (that merge in $z \leq 1$) when their GW frequency $f_{\text{GW}} = 10$ and 10^{-4} Hz by e_1 and e_{-4} , respectively. N_{merge} denotes the number of BBH mergers. All numbers with error-bars denote the mode and 1σ range for the respective distributions.